

Supporting Information

Perylene bisimide network for high-performance n-type electrochromism

Weitao Ma,^a Leiqiang Qin,^a Yu Gao,^b Wenqiang Zhang,^b Zengqi Xie,^{*a} Bing Yang,^b
Linlin Liu^a and Yuguang Ma^{*a}

^a Institute of Polymer Optoelectronic Materials and Devices, State Key Laboratory of Luminescent Materials and Devices, South China University of Technology, Guangzhou 510640, P. R. China. E-mail: msxiez@scut.edu.cn; ygma@scut.edu.cn.

^b State Key Laboratory of Supramolecular Structure and Materials, Jilin University, Changchun 130012, P. R. China.

Table of contents:

1. Experimental section·····	S2
2. Synthesis of PBI monomer·····	S4
3. Optical properties of Cl-PBI and PO-PBI·····	S7
4. FT-IR and UV spectrum of electropolymerized film·····	S8
5. Morphology and stability of EP films·····	S10
6. Electrochemical properties·····	S11
7. DFT theoretical calculation·····	S17

1. Experimental Section

Materials and Methods. Solvents and reagents were purchased from commercial sources and were used as received, unless otherwise stated. All the reagents and solvents were used as received or purified using standard procedure. Column chromatography was performed with silica gel (HaiYang Silica 60, particle size 0.035-0.070 mm). ^1H and ^{13}C NMR were recorded using a Bruker-300 spectrometer operating at 500 and 75 MHz in deuterated chloroform solution at 298 K. Chemical shifts were reported as δ values (ppm) relative to an internal tetramethylsilane (TMS) standard. The UV-vis absorption and fluorescence spectra were recorded on a Shimadzu UV-3600 and spectro-photometer, respectively. Cyclic voltammetry (CV) measurement was performed on a CHI600D electrochemical workstation. Atomic force microscopy (AFM) measurement was carried out using a Digita Instrumental DI Multimode Nanoscope IIIa in tapping mode.

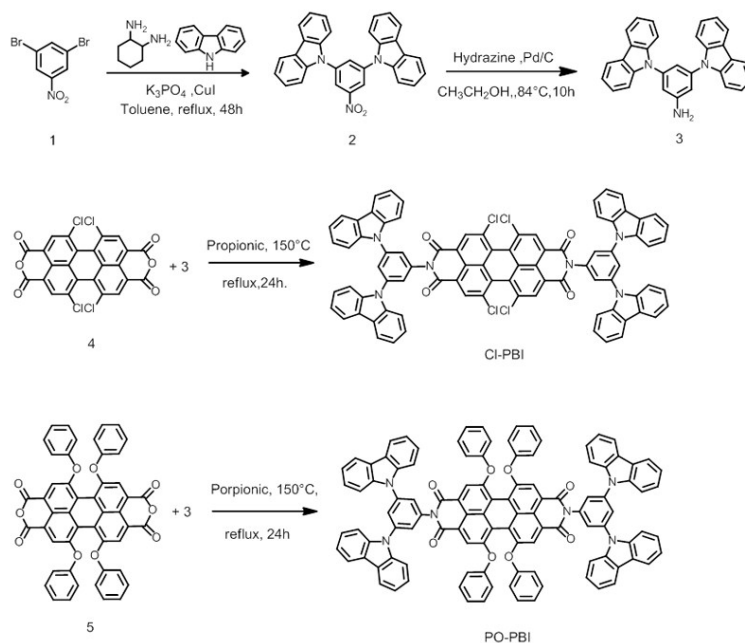
All the electro-generated films used in the electrochemical and electrochromic experiments were fabricated by CV method for 20 cycles (38nm) under the following conditions. The Ag/Ag⁺ electrode with AgNO₃ (0.01 M) in acetonitrile was used as reference electrode. The monomer (0.15 mg /mL) was dissolved in the mixture of CH₃CN and CH₂Cl₂ ($V_{\text{CH}_3\text{CN}} / V_{\text{CH}_2\text{Cl}_2} = 3:2$) together with Bu₄NPF₆ (0.1 M) as the supporting electrolyte. ITO was used as the working electrode and titanium metal was used as the counter electrode. The scanning rate was 100 mV s⁻¹. The film thickness was measured by Veeco dektall50 Level gauge instrument.

The spectroelectrochemistry and square-wave potential step absorptiometry experiments were conducted in a quartz cell located in the UV-3600 instrument under ambient circumstance. The Ag electrode was used as reference electrode and platinum was used as counter electrode and electro-generated film on ITO glass as work electrode.

The High Performance Liquid Chromatography (HPLC) was characterized on the JAI LC-9230NEXT instrument using HPLC pure dichloromethane as mobile phase. The chromatographic column was JAIGEL SIL normal phase column. The detector was UV-600NEXT. The flow rate was 10 mL/min. The absorbance data detected at

wavelength of 520/560 nm for Cl-PBI/PO-PBI was adopted to obtain spectra as presented in Synthesis section.

2. Synthesis of PBI monomer



Scheme S1. Synthetic route of Cl-PBI, PO-PBI

3, 5-dicarbazol-nitrobenzene (compound 2):

A mixture of 1, 3-dibromo-5-nitrobenzene (2.8 g, 10.0 mM), carbazole (3.34 g, 20.0 mM, 200 mol %), CuI (380 mg, 10 mol %), trans-1, 2-diaminocyclohexane (460 mg, 20 mol %), K_3PO_4 (8.9 g, 210 mol %) and 80 mL toluene was heated at 110 °C for 24 hours under nitrogen. After cooling to room temperature, the mixture was quenched with distilled water, and then the precipitate was extracted with dichloromethane. The organic phase was dried over anhydrous magnesium sulphate. After evaporation of the solvent, the residue was purified by column chromatography eluting with mixed solvent (petroleum ether: dichloromethane = 3:1) to give a fluffy yellow solid (2.54 g). Yield: 55%. 1H NMR ($CDCl_3$, 500 MHz, 298K, TMS) δ 8.57 (d, 4H), δ 8.42 (t, 2H), δ 8.30 (d, 8H), δ 7.70 (d, 8H), δ 7.5 (t, 8H), δ 7.36 (t, 8H).

3, 5-dicarbazol-aniline (compound 3):

The reaction of 3, 5-dicarbazol-nitrobenzene (compound 2) (2 g, 4.45 mM), 80% hydrazine hydrate (5ml), 10% Pd/C (75 mg) and 80 ml ethanol reflux at 84 °C for 10

hours under nitrogen yielded compound 3 (1.85 g). Yield: 99%. ¹H NMR (DMSO, 300 MHz, 298K, TMS) δ 8.23 (d, 8H), δ 7.61 (d, 8H), δ 7.47 (t, 8H), δ 7.29 (t, 8H), δ 6.94 (s, 2H), δ 6.86 (s, 1H), δ 5.89 (s, 2H).

Cl-PBI:

A mixture of tetrachlorinated 3, 4:9, 10-perylenetetracarboxylic dianhydride 4 (0.398 mg, 0.75 mM), compound 3 (0.64 g, 1.5 mM) and 15 ml propionic acid was heated at 150 °C for 24 h. After cooling to room temperature, the mixture was washed with water and methanol, dried in a vacuum oven. The residue was purified by column chromatography eluting with mixed solvent (petroleum ether: dichloromethane = 1:3) to give a deep red solid (457.51 mg). Yield: 85.7%. ¹H NMR (CDCl₃, 300 MHz, 298K, TMS) δ 8.85 (s, 4H), δ 8.15 (d, 8H), δ 8.05 (s, 2H), δ 7.75 (m, 12H), δ 7.5 (t, 8H), δ 7.35 (t, 8H); ¹³C NMR (CDCl₃, 75 MHz, 298K, TMS): 162.10, 140.30, 140.0, 136.70, 135.0, 133.58, 131.70, 129.15, 126.40, 125.85, 124.60, 123.80, 123.50, 123.19, 120.63, 120.48, 109.93 ppm; MALDI-TOF (m/s): calcd. for C₈₄H₄₂Cl₄N₆O₄ 1340.204; found, 1340.273.

PO-PBI:

Tetraphenoxy-substituted 3,4:9,10-perylenetetracarboxylic dianhydride 5 was prepared according to the method of similar perylenetetracarboxylic dianhydride as reported. A mixture of tetraphenoxy-substituted 3,4:9,10-perylenetetracarboxylic dianhydride 5 (0.5 mg, 0.65 mM), compound 3 (0.68 g, 1.6 mM) and 20 mL propionic acid was heated at 150 °C for 24 h. After cooling to room temperature, the mixture was washed with water and methanol, dried in vacuum oven. The residue was purified by column chromatography eluting with mixed solvent (petroleum ether: dichloromethane = 1:3) to give an amaranth solid (377.8 mg). Yield: 38%. ¹H NMR (CDCl₃, 300 MHz, 298K, TMS) δ 8.24 (s, 4H), δ 8.0 (d, 8H), δ 7.8 (s, 2H), δ 7.56 (d, 4H), δ 7.54 (d, 8H), δ 7.36 (t, 8H), δ 7.2 (m, 16H), δ 7.05 (t, 4H), δ 6.9 (d, 8H); ¹³C NMR (CDCl₃, 75 MHz, 298K, TMS): 162.10, 155.028, 154.236, 139.35, 139.30,

138.69, 136.43, 132.11, 129.05, 128.01, 127.20, 125.33, 125.25, 123.75, 122.65, 121.50, 120.03, 119.50, 119.36, 119.0, 118.88 ppm; MALDI-TOF (m/s): calcd. for $C_{108}H_{62}Cl_4N_6O_8$ 1571.476; found, 1571.647.

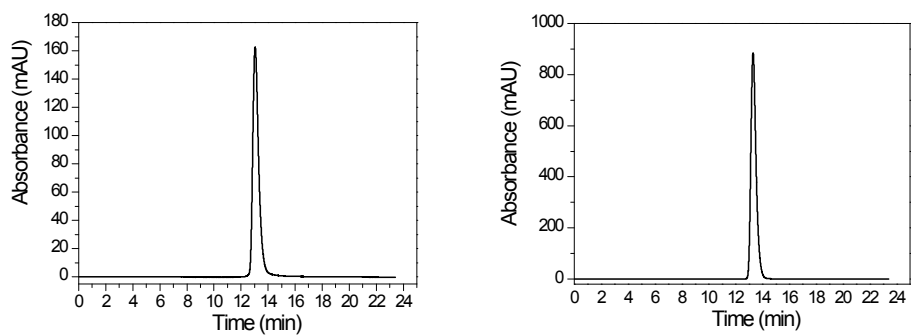


Figure. HPLC spectrum of the Cl-PBI (left) and PO-PBI (right).

3. Optical properties of Cl-PBI and PO-PBI

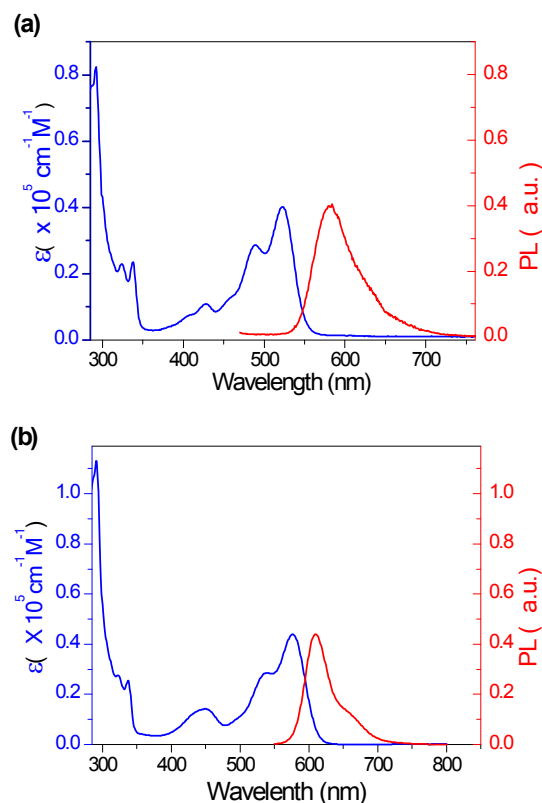


Figure S1. Optical properties of two monomers. (a) absorption and PL spectra of Cl-PBI and PO-PBI (b) in dichloromethane ($c = 1 \times 10^{-5} \text{ M}$). The two monomers were soluble in common solvents such as dichloromethane, chloroform, chlorobenzene, and toluene. The absorption and emission properties of Cl-PBI and PO-PBI in diluted dichloromethane solution were investigated by UV/Vis and fluorescence spectroscopy, as shown in Figure S1. The two monomers showed strong absorption in visible light region with absorption maxima at 520 nm and 575 nm in CH_2Cl_2 correspondingly which corresponded to the S_0 – S_1 of the perylene core. Quite similar to most of the bay-area substituted perylene bisimides, both two compounds presented a mirror relationship between the emission and absorption spectra with a Stokes shift of 60 nm and 33 nm accordingly.

4. FT-IR and UV spectrum of electropolymerized film

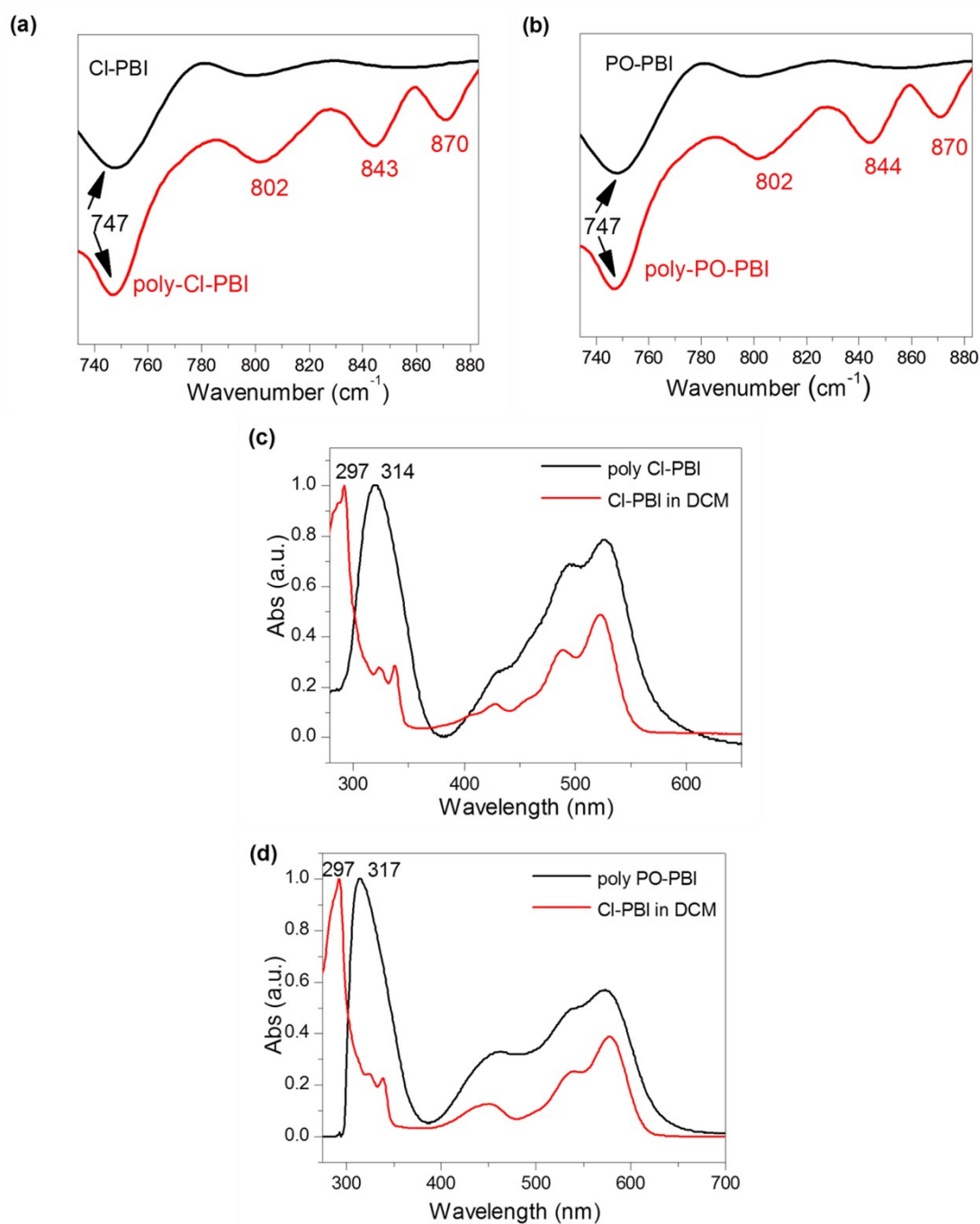


Figure S2. FT-IR and UV spectrum of EP film. (a)/ (b) FT-IR spectra of Cl-PBI, PO-PBI and its EP film. (c)/ (d) Normalized UV-vis absorption spectra of spin-coated film and EP film. As the FT-IR spectra showed, there were some new-generated peaks for corresponding EP films. The peak at 747 cm⁻¹ is attributed to the carbazole ring. The peaks at 802 cm⁻¹, 843, cm⁻¹, 870 cm⁻¹ in EP film were attributed to the tri-substituted carbazole ring. This indicated the polymerization occurred between the carbazoles

and the formation of polycarbazole. The bathochromic shift of carbazole from 297 nm to 317 nm were also observed in UV-vis spectra, which indicated the formation of polycarbazole as well. These observations in FT-IR spectra indicated the high coupling efficiency between carbazole groups and the formation of cross-linked film. The absorption spectra also revealed the separation of the carbazole and PBI core, which ensures their independent functions, i.e. electrochemical coupling from carbazole moieties and electrochromism from PBI core that given in the communication context.

5. Morphology and stability of EP films

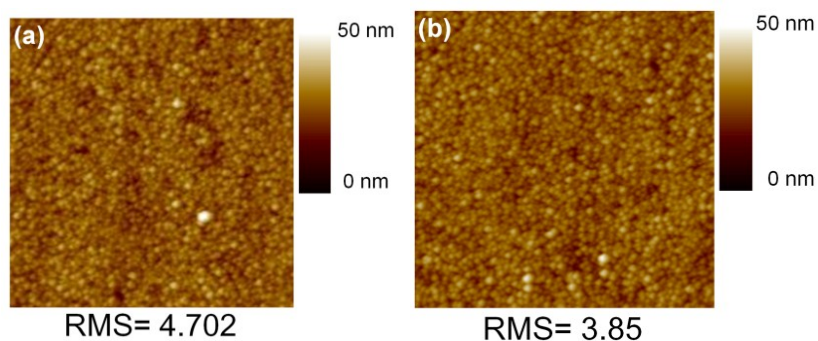


Figure S3. AFM morphology of two EP films. (a) poly Cl-PBI films for 20 cycles. (b) poly PO-PBI EP film for 20 cycles. The size of the images was 5 μm×5 μm. The films were prepared under the condition as: 0.1 mg /mL monomer, 0.1 M Bu₄NPF₆, mixed solvents V_{CH₃CN} : V_{CH₂Cl₂} = 3:2, scanning rate was 100 mV s⁻¹. The two EP films showed typical domain-like morphology as previously reported electrochemical-generated films.

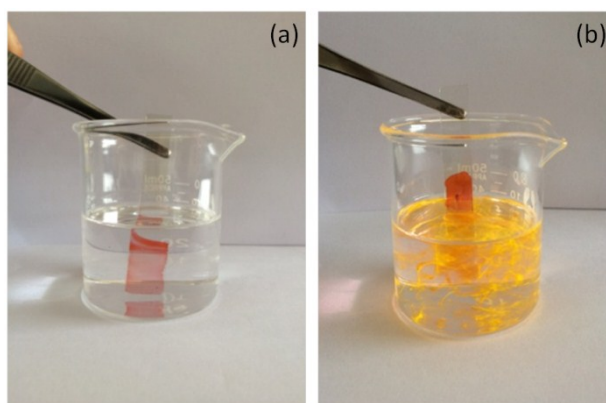


Figure S4. (a) Cross-linked poly-Cl-PBI film sunk in dichloromethane. (b) Spin-coated thin film of Cl-PBI sunk in dichloromethane.

6. Electrochemical properties

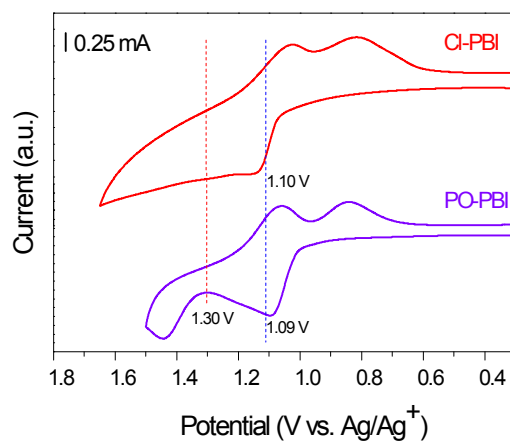


Figure S5. Electrochemical properties of different moieties in two poly-PBI films. CV curves of Cl-PBI, PO-PBI in solution at a scan rate of 50 mVs^{-1} for the first cycle. In order to experimentally determine the conditions for the electropolymerization, we investigated the electrochemistry of the Cl-PBI and PO-PBI. As shown in Figure S5, in the anodic sweep a peak at +1.10 V (oxidation onset is $\sim 1.0 \text{ V}$) nearby was assigned to the formation of carbazole radical cations that is lower than the oxidation potential of PBI core ($> +1.3 \text{ V}$).

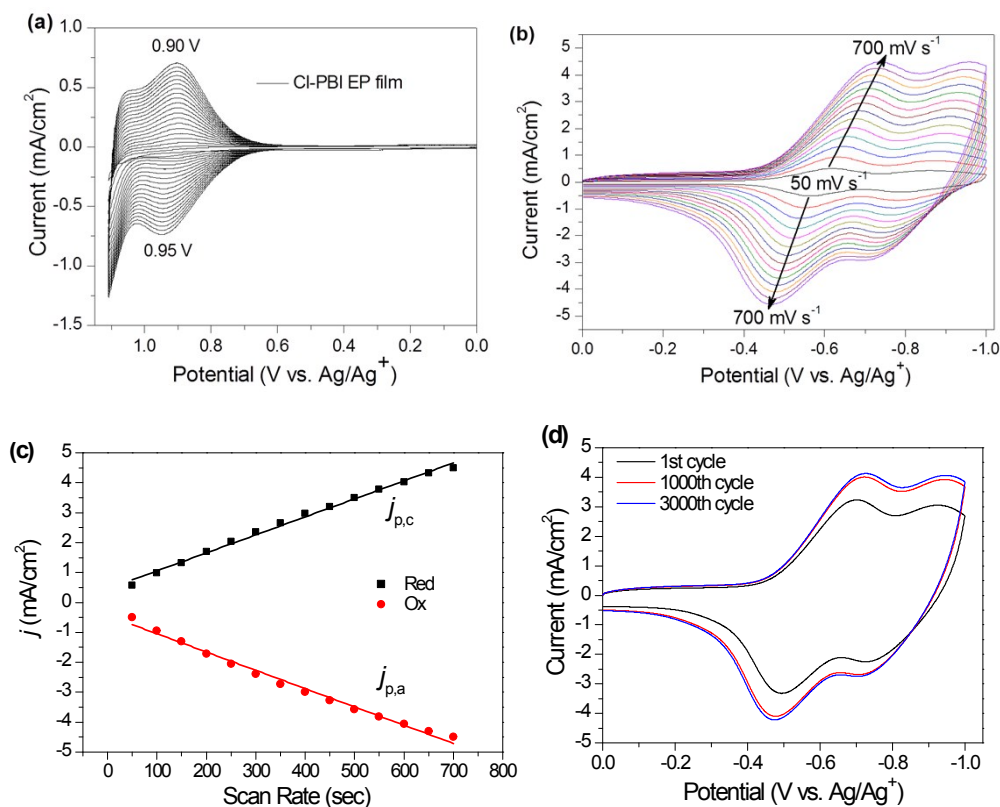


Figure S6. Electrochemical properties of poly-Cl-PBI film. (a) *In situ* electropolymerization of Cl-PBI using CV method at a scan rate of 100 mV s^{-1} for 20 cycles. (b), (c) Scan-rate dependence of the poly-Cl-PBI film in CH_3CN containing Bu_4NPF_6 (0.1 M) at different scan rates between 50 and 700 mV s^{-1} . Interval scan rate: 50 mV s^{-1} . (c) Cyclic voltammograms of poly-Cl-PBI film upon repeated cycling at the rate of 150 mV s^{-1} at the potential range from -1.0 V to 0 V in CH_3CN containing 0.1 M Bu_4NPF_6 . To avoid the influence on PBI moiety during the electropolymerization process, the PBI-based network films were fabricated by cyclic voltammetry (CV) in the potential range of $0 \sim +1.13 \text{ V}$ with a scan rate of 100 mV s^{-1} . During the successive scanning cycles, in anodic sweeps a couple of newly generated dimeric carbazole redox peaks at the low potentials of +0.95 V (oxidation peak) and +0.90 V (reduction peak) were observed and the peak current increased step by step, indicating that more and more dimeric carbazole units were created on the surface of the electrode.

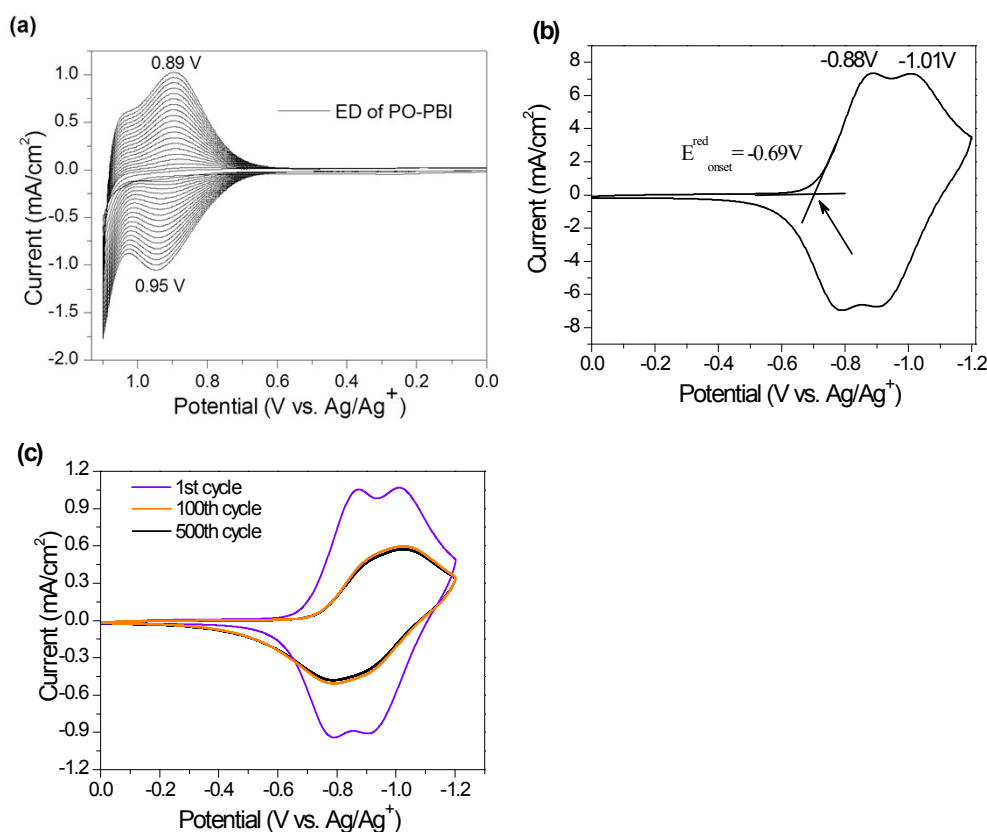
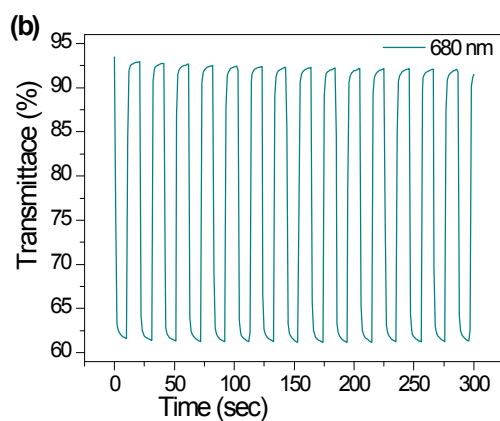
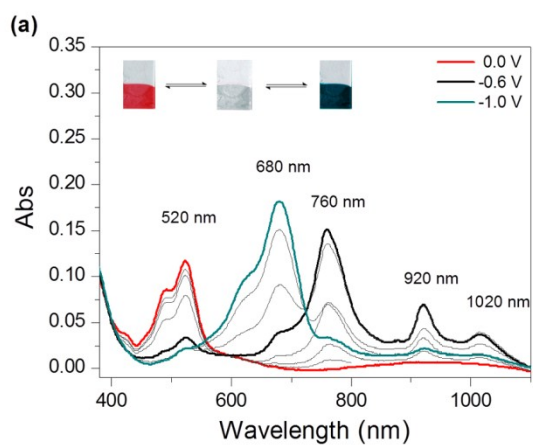


Figure S7. Electrochemical properties of poly-PO-PBI film. (a) *In situ* electropolymerization of PO-PBI using CV method at a scan rate of 100 mV s^{-1} for 20 cycles. (b) The electrochemical reduction behavior of poly-PO-PBI film at a scan rate of 50 mV s^{-1} . (c) Cyclic voltammograms of poly-Cl-PBI film upon repeated cycling at the rate of 150 mV s^{-1} at the potential range from -1.2 to 0 V in CH_3CN containing $0.1 \text{ M Bu}_4\text{NPF}_6$. Similarly, the PO-PBI based net-work was also fabricated by CV method in the potential range of $0 \sim +1.13 \text{ V}$. During the successive scanning cycles, in anodic sweeps a couple of newly generated dimeric carbazole redox peaks at the low potentials of $+0.95 \text{ V}$ (oxidation peak) and $+0.89 \text{ V}$ (reduction peak) were observed and the peak current increased step by step, indicating that more and more dimeric carbazole units were created on the surface of the electrode. The CV curves of PO-PBI was almost the same as that of Cl-PBI and this similarity can be attribute to the separation effect of the notes at nitrogen atoms. The poly-PO-PBI film presented two reduction peaks as well when reduced ($-1.2 \rightarrow 0 \text{ V}$, vs Ag/Ag^+). The cyclic stability of poly-PO-PBI film was investigated at the potential range of -1.2 V to 0 V and it showed inferior stability compared with its counterpart poly-Cl-PBI film with about

60.2% electrochemical activity remaining only after 500 cycles. Obviously, the poly-PO-PBI film exhibited inferior electrochemical stability compared with the poly-Cl-PBI film.



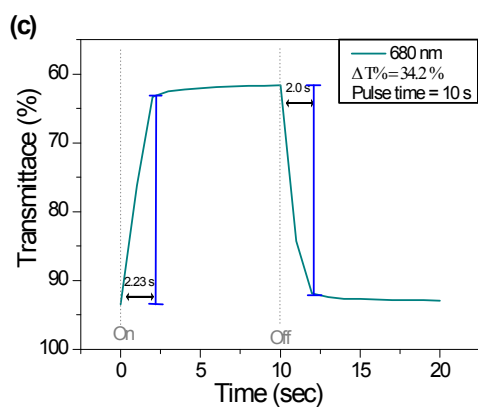
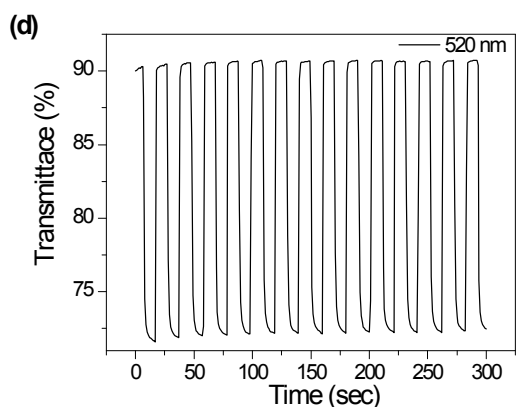


Figure S8. Electrochromic switching of poly-Cl-PBI film. Gradient spectrochemistry of the poly-Cl-PBI film on ITO-coated glass in CH_3CN containing 0.1 M Bu_4NPF_6 at various applied potential (*vs.* Ag/Ag^+) for (a). Square-wave potential step absorptometry of poly-Cl-PBI film (monitored at 680 nm for (b) and 520 nm for (c) $-1.0 \text{ V} \rightarrow 0.0 \text{ V}$ versus Ag/Ag^+). Calculation of optical switching time at 680 nm (d), 520 nm (e) and 760 nm (f).

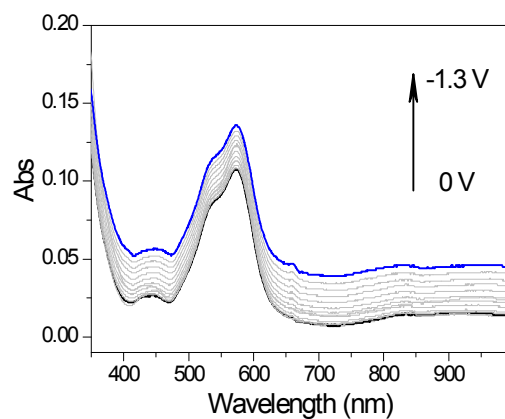


Figure S9. Electrochromic switching of poly-PO-PBI films. Spectrochemistry of the poly-PO-PBI film on ITO-coated glass in CH_3CN containing 0.1 M Bu_4NPF_6 at various applied potential (vs. Ag/Ag^+).

7. DFT theoretical calculation

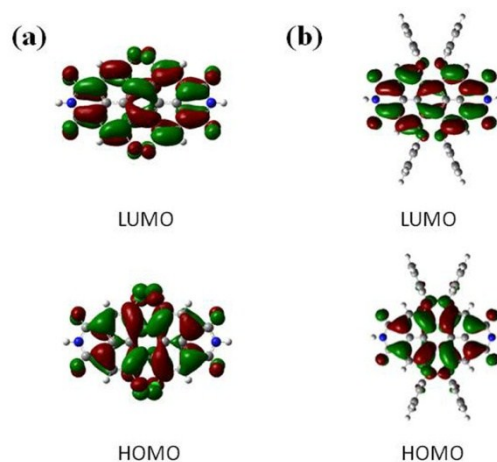


Figure S10. The HOMO and LUMO for PBI part. The HOMO and LUMO of PBI part of Cl-PBI (a) and PO-PBI (b). Note that both frontier orbitals exhibit nodes at the imide nitrogens of the two molecules. The geometry optimizations for the ground state of the neutral PBI part molecules of Cl-PBI and PO-PBI were performed using density functional theory (DFT) with the B3LYP hybrid functional and 6-31+G (d, p) basis set in a close shell.

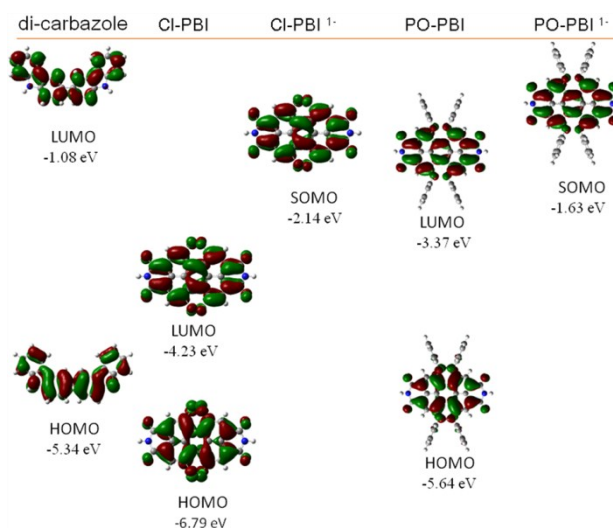


Figure S11. The frontier orbitals of different part in poly-PBI films. The frontier orbitals of di-carbazole and Cl-PBI, Cl-PBI¹⁻, PO-PBI, PO-PBI¹⁻. The LUMO energy of di-carbazole was higher than that of Cl-PBI, PO-PBI, which meant one extra electron would locate on PBI part. Similarly, the LUMO energy of di-carbazole was also higher than the SOMO of both Cl-PBI¹⁻ and PO-PBI¹⁻, which meant the second

extra electron would locate on PBI as well. It was noteworthy that the LUMO of both neutral Cl-PBI form and its anion form were lower than that of PO-PBI. Thus, theoretical calculation also verified that the reduction of poly-Cl-PBI was easier than that of poly-PO-PBI.

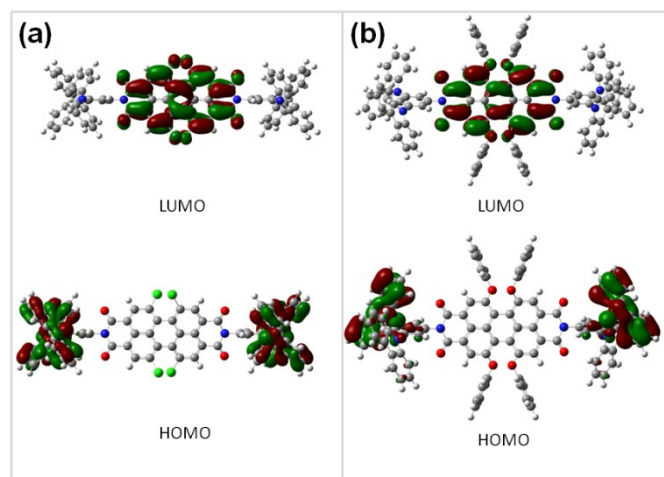


Figure S12. The HOMO and LUMO for two PBI precursors. The frontier molecular orbitals of (a) Cl-PBI and (b) PO-PBI. Density functional theory (DFT) calculation (B3LYP/6-31+G(d, p) method) was also implemented to analysis the entire frontier molecular orbitals, and the results indicated that the highest occupied molecular orbitals (HOMOs) locate at carbazole units and the lowest unoccupied molecular orbitals (LUMOs) locate at PBI parts, as shown in Figure S12. Such totally separated frontier molecular orbitals in the monomers are thanks to the nodes of the imide nitrogen (Figure S10) as mentioned above, which facilitates the separation of the functions of the carbazole units and the PBI cores, i.e. electrochemical coupling from carbazole moieties and electrochromism from PBI core.